



Electrochemical detection of glucose at physiological pH using gold nanoparticles deposited on carbon nanotubes

David Branagan, Carmel B. Breslin*

Department of Chemistry, Maynooth University, Maynooth, County Kildare, Ireland

ARTICLE INFO

Keywords:

Carbon nanotubes
Gold nanoparticles
Nanocomposite
Glucose sensor
non-enzymatic
Physiological pH

ABSTRACT

There is currently considerable interest in the development of non-enzymatic glucose sensors and gold is one of the noble metals that enables the oxidation of glucose. Gold nanoparticles with a mean diameter of 7.5 nm were deposited onto the walls of functionalised carbon nanotubes to give a gold loading of 2.0% by weight. This composite was dispersed and cast onto glassy carbon and carbon screen printed electrodes. These electrodes were then used to detect glucose in a neutral phosphate buffer solution, corresponding to physiological pH. Using constant potential amperometry, a linear calibration curve was obtained with a sensitivity of $2.77 \pm 0.14 \mu\text{A}/\text{mM}$, a limit of detection, LOD, of $4.1 \mu\text{M}$ and a linear region extending to 25 mM. This sensor showed very good selectivity in the presence of ascorbic acid, galactose and fructose, but interference was observed in the presence of uric acid. This interference was eliminated by applying a Nafion® film to the composite electrodes. Due to a lower diffusion of glucose across the Nafion® barrier, the sensitivity of the Nafion® coated composite was reduced to $0.55 \pm 0.03 \mu\text{A}/\text{mM}$ and the LOD was increased to $10.0 \mu\text{M}$. However, a linear response between 0.1 mM and 25 mM was obtained, which covers the normal and elevated levels of glucose in blood. These sensors showed very good stability when stored in air and it was also possible to re-use the sensors.

1. Introduction

Enzyme-based glucose sensors, where an enzyme is immobilised onto an electrode surface, are well known and they have been used in point-of-care applications and in the diagnosis and management of diabetes [1–3]. Although enzymes normally have excellent specificity towards the target biomolecule, they can sometimes become inactive. The bioactivity of the enzyme may be reduced during immobilisation and further lowered as the sensor is stored [4]. The enzymes employed in glucose sensors are typically glucose oxidase (GOx) and glucose dehydrogenase (GDH) and these can exhibit degradation when exposed to hydrogen peroxide and other low molecular weight species, such as ascorbate or urate [4,5]. Due to the issues with oxygen dependency seen in the first generation glucose sensors, various synthetic redox active mediators were developed and used in second generation sensors, while third generation sensors are based on the direct electron transfer between the enzyme and the electrode surface, thereby bypassing the need for a mediator or oxygen [4,6]. Nevertheless, these sensors remain susceptible and prone to enzyme degradation.

An alternative approach that has gained interest in recent years is the development of non-enzymatic glucose sensors [1]. The non-enzymatic glucose sensors are generally focussed on noble metals with

gold being of particular interest, as it shows good electroactivity towards the oxidation of glucose [7–9]. It has excellent biocompatibility compared to some of the bimetallic or alloy combinations, such as PdCu, PtAu, PdAu, CuO, NiO and NiOPt, that have been studied [10,11] and contain heavy metal elements. It is also more superior than platinum that suffers from poisoning from adsorbed intermediates [12]. Furthermore, gold can be employed as nanoparticles, or other nanostructures, that are relatively easy to synthesise [13–15].

Although the oxidation of glucose at gold in alkaline solutions is well described, the mechanism governing this electron-transfer reaction is not fully understood. It is known that the chemisorption of hydroxide anions provides a more favourable interaction between glucose and the gold substrate and this facilitates the oxidation reaction. The hydroxide anions neutralise the anomeric hydrogen atom that is eliminated during the initial formation of adsorbed intermediates. Furthermore, $\text{Au}(\text{OH})_{\text{ads}}$, which is generated in this alkaline environment, is believed to be catalytically active towards the oxidation of glucose [1,7]. Therefore, it is no surprise that the non-enzymatic glucose sensors are mostly focused on alkaline environments, with most of the studies being carried out in a 0.1 M NaOH solution [14,15]. In order to further improve the electroactivity and sensitivity of gold in the detection of glucose, gold nanoparticles are commonly employed

* Corresponding author.

E-mail address: Carmel.Breslin@mu.ie (C.B. Breslin).

<https://doi.org/10.1016/j.snb.2018.11.089>

Received 14 June 2018; Received in revised form 25 October 2018; Accepted 18 November 2018

Available online 19 November 2018

0925-4005/ © 2018 Elsevier B.V. All rights reserved.

[14–16]. They have been combined with a number of other materials, and composites comprising gold nanoparticles and carbon nanotubes are attracting a lot of attention. For example, a number of recent reports have been published on the use of gold nanoparticles, or gold nanoparticles combined with carbon-based materials, such as carbon nanotubes or graphene, for the electrochemical detection of glucose in alkaline solutions [14–19]. Good linear ranges, typically extending to glucose concentrations of 1–20 mM with low detection limits in the vicinity of 0.5–5.0 μM , have been reported for these sensors in alkaline solutions [14–19].

It is more challenging to detect glucose at gold containing composites in neutral solutions, where the concentrations of OH^- and $\text{Au}(\text{OH})_{\text{ads}}$ species are considerably lower. However, a non-enzymatic glucose sensor that can detect glucose at physiological pH has advantages, as there is no need to modify the pH of the glucose-containing solution prior to analysis. In this paper, we show that it is possible to detect glucose in a neutral buffered solution, maintained at physiological pH values, using electrodes modified with gold nanoparticles and carbon nanotubes. The carbon nanotubes were employed to support the gold nanoparticles as they have excellent conductivity and a high surface area. Furthermore, they are readily functionalised with carboxylic acid groups and at neutral pH these groups are dissociated to give anionic surface groups that may assist in repelling anionic interferences, such as ascorbate and urate. As detailed earlier, gold nanoparticles combined with carbon-based materials have previously been used to detect glucose in alkaline solutions [14–19]. In this study physiological pH values are employed, the influence of several interferences on the glucose signal is investigated and the stability and selectivity of the sensor is improved using a Nafion[®] film.

2. Experimental

Multi-walled carbon nanotubes (MWCNTs > 99% purity) and all other reagents were purchased from Sigma Aldrich. The pristine MWCNTs were purified and modified with carboxylated groups to increase their dispersion in solution by refluxing in concentrated HNO_3 at 120 °C for 24 h. The resulting functionalised nanotubes, fn.MWCNTs, were extracted from the acid and purified using centrifugation with repeated cycles of dilution with deionised water until the pH was neutral. Then, the fn.MWCNTs were isolated on a 0.45 μm membrane and washed thoroughly with deionised water. Gold nanoparticles were deposited at the fn.MWCNTs using citrate or borohydride as a reducing agent. The functionalised carbon nanotubes were dispersed into a 1% sodium dodecyl sulfate (SDS) solution at a concentration of 0.5 mg/mL, using ultra-sonication to yield a homogeneous and stable dispersion. The gold nanoparticles were formed by adding, with stirring, a 1% w/v $\text{HAuCl}_4 \cdot 3\text{H}_2\text{O}$ solution and then slowly adding a 0.75% w/v NaBH_4 solution. After 5 min, the resulting composite material was isolated. The gold particles were formed from the citrate solution using a similar process, where the functionalised carbon nanotubes were first mixed with the $\text{HAuCl}_4 \cdot 3\text{H}_2\text{O}$ to facilitate adsorption of gold ions onto the carbon nanotubes. Then the solution was diluted to 0.25 mg/mL and heated to 100 °C and a hot 1.0% trisodium citrate solution was added and the mixture was left to reflux for 5 min. The final composite materials were fully dried using an infrared lamp and stored in a desiccator.

The glucose sensors were fabricated by firstly dispersing the composites, 4 mg/mL, in a 1% SDS solution. Then 5 μL of this dispersion was cast onto a glassy carbon electrode (3 mm) or 10 μL onto a screen printed electrode (due to the higher surface area) and left to dry under an infrared lamp. The SDS was removed by cycling the modified electrodes in 0.3 M NaOH at 100 mV s^{-1} between -0.40 V and 0.60 V vs. SCE for the glassy carbon electrodes and between -0.60 and 0.40 V vs. Ag/AgCl for the screen printed electrodes. The concentration of SDS in the solution was monitored using UV–Vis spectroscopy and cycling was continued until the absorbance of the SDS remained constant, which

was determined as approximately 50 cycles. Then the electrodes were cycled in a 0.1 M PBS solution followed by a cleaning step in 1.0 M H_2SO_4 , by cycling at 100 mV s^{-1} between 0.0 V and 1.40 V vs. SCE for glassy carbon and between -0.20 V and 1.20 V vs. Ag/AgCl for the screen printed electrodes. These potential limits were selected (after several experiments where the limits were varied) to optimise the detection of glucose. Following this final cleaning step, the composites were cycled in the PBS solution until steady-state conditions were obtained. Nafion[®] coatings were applied to the composite using a drop cast method. The Nafion[®] 117 solution was diluted by 50% in ethanol. A 3 μL volume was cast over the composite and the composite was allowed to dry at room temperature.

The composites were characterised using a FEI Titan TEM and a Hitachi S–3200–N SEM, energy dispersive X-Ray analysis (EDX) with an Oxford Instrument INCAx-act EDX system. For the TEM measurements, the composite was dispersed in ethanol and 20 μL of this mixture was left to dry on a carbon support on a copper grid. A statistical analysis on the size of the nanoparticles was conducted on 100 random gold particles using IMAGE J software. X-Ray diffraction (XRD) was conducted on a PANalytical X'Pert PRO MPD system. A Perkin Elmer Precisely Analyst system was used for atomic absorption spectroscopy (AA). Raman spectra were recorded using a LabRAM high resolution Raman spectrometer at 600 nm. All samples were prepared in KBR discs. Cyclic voltammetry was carried out on a Solartron SI 1287 potentiostat and constant potential amperometry experiments were performed with a CH Instruments CHI 760C potentiostat. Initial studies were performed with a conventional three-electrode cell, consisting of a high surface area platinum counter electrode, a saturated calomel reference electrode (SCE) and the modified glassy carbon (GC) electrode. The screen printed electrodes (SPE) were obtained from Metrohm (DRP–150) and consisted of a printed carbon working electrode and a platinum counter electrode. The original silver reference electrode was converted to a silver–silver chloride reference (Ag/AgCl) using a high concentration of FeCl_3 in deionised water until a dark purple–grey colour was achieved. Ultra-pure water obtained through a Millipore filtration system was used in all experiments. A 0.1 M phosphate buffer solution (PBS) at a pH of 7.4 was used in all electrochemical studies.

A quantification of the surface acid groups introduced during refluxing in HNO_3 was obtained using an acid base titration. The fn.MWCNTs were dispersed in a standardised 0.01 M NaOH solution in 0.1 M NaCl and left to stir for 14 h under N_2 bubbling to displace adsorbed CO_2 from the fn.MWCNTs. The amount of gold in the composites was measured using AA. The gold was extracted using *aqua regia* to yield a yellow coloured HAuCl_4 solution which was isolated in 0.1 M HCl. Standard solutions were prepared from a commercial 1000 ppm standard stock solution, which consisted of 1.00 mg of pure gold in 15% HCl.

3. Results and discussion

Prior to the detection of glucose the fn.MWCNT–Au_{nano} composites were characterised to obtain information on the percentage of acidic groups introduced during the acid functionalisation, the size, distribution and crystallinity of the gold nanoparticles and the amount of gold deposited at the carbon nanotubes.

3.1. Characterisation of composites

Typical acid–base titration curves are shown in Fig. 1, where the titration curves obtained using pristine MWCNTs and fn.MWCNTs are compared. Two equivalence points (EP) are clearly visible during the titration of the fn.MWCNTs, while a single EP is seen with the pristine MWCNTs. The EP at approximately a pH of 8.0 is related to the total surface acidity, while the EP at a pH of about 5.0 is associated with surface adsorbed polycyclic carbonaceous fragments, which become de-adsorbed and appear in the NaOH filtrate as carboxylic salts [20].

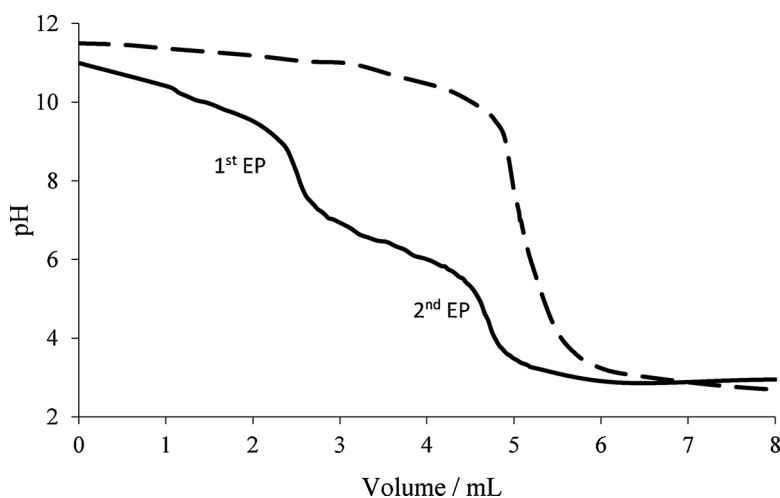


Fig. 1. Potentiometric titrations of — — — pristine MWCNTs and — fn.MWCNTs.

Using these data, the acidic group coverage was calculated as 6% for the fn.MWCNTs, whereas the pristine MWCNTs yielded no indication of any acidic functionalities. The presence of carboxylic groups at the fn.MWCNTs was confirmed using FTIR, where a peak at 1725 cm^{-1} was observed and attributed to the stretching mode of the carbonyl group.

Representative TEM micrographs are shown for the fn.MWCNT–Au_{nano} prepared using the citrate and borohydride reducing agents at different magnifications in Fig. 2(a)–(c) while distributions of the gold particles with different diameters are shown in the accompanying size distribution plots, Fig. 2(d) and (e). The gold particles appear to be reasonably well dispersed along the carbon nanotubes, with the borohydride reducing agent, Fig. 2(a) and (c), and they appear to exist in the nanoscale region with the majority below 10 nm in diameter with no evidence of particle agglomeration. The size distribution histogram, Fig. 2(d), shows the distribution ranging from 5.5 to 12.5 nm in diameter, with a mean diameter of 7.5 nm. On the other hand, the particles prepared using the citrate system appear in groups, with doublets, triplets and higher groupings, Fig. 2(b). This shows that the nucleation of new particles occurs at the existing gold particles rather than at new sites on the carbon nanotubes. Much larger nanoparticles are formed with the average diameter of 23 to 24 nm, as evident in Fig. 2(e). The data presented in Fig. 2(f) show the lattice fringes of a gold nanoparticle. By measuring the distance between these fringes, the inter-atomic spacing was measured as 2.35 Å which corresponds to the (111) plane of crystalline gold.

A typical XRD spectrum of the fn.MWCNT–Au_{nano} generated using borohydride is presented in Fig. 3, where the crystalline planes are evident and these are shown on the figure. The reflection at $2\theta = 25.84^\circ$ corresponds to the (002) graphitic plane of the carbon nanotubes, while those appearing at 38.23° , 44.50° , 64.64° , 77.52° , and 81.60° correspond to the (111), (200), (220), (311) and (222) planes, respectively, of the crystalline gold particles [21,22]. It is clear that the (111) plane is the most abundant and these data indicate that the gold particles are formed predominantly with a face centred cubic structure. The size of the gold particles was estimated using the Scherrer equation, Eq. 1, where D is the average diameter of a spherical particle, β is the full width at half maximum of the most intense reflection, θ is the position of the reflection, λ is the wavelength and 0.89 is the Scherrer constant [23]. Using this approach, the diameters of the gold particles were estimated at 7.92 nm with borohydride and 20.29 nm with citrate. These values agree well with the TEM results, Fig. 2.

$$D = \frac{0.89\lambda}{\beta \cos \theta} \quad (1)$$

Using AA and EDX the gold loading in the fn.MWCNT–Au_{nano} was estimated. Although EDX is not a quantitative technique, it was used in

combination with the AA data. Using the EDX data, the % weight of C, O and Au was calculated and these data were used to obtain an approximate gold loading of 2.8%. A more accurate loading of 2.0% was obtained using AA spectroscopy. As expected a higher loading of approximately 5.0% was obtained with the citrate system.

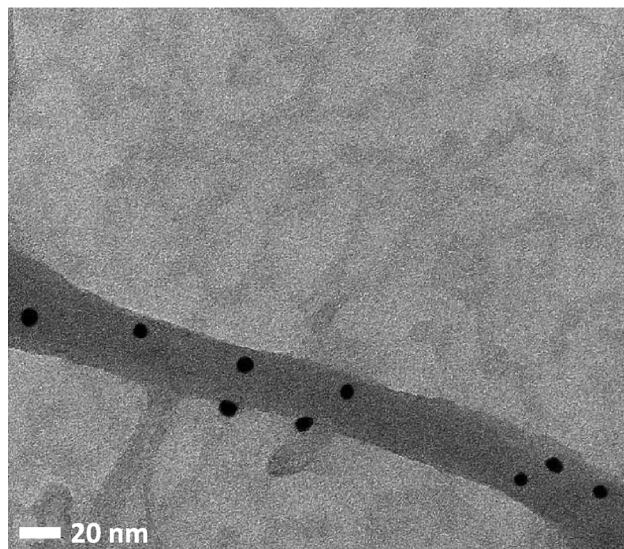
In Fig. 4, RAMAN spectra are shown for the fn.MWCNT and fn.MWCNT–Au_{nano} composite. Distinctive G and D bands can be seen which arise from C–C stretching vibrations within the hexagonal sp^2 hybridised graphitic rings and the vibrations of these graphitic rings in the presence of symmetry-containing defects, respectively. At a higher frequency, another peak arises which can be assigned as a disorder induced peak, termed D', which is usually proportional to the acid reflux time [24]. The bands of the fn.MWCNTs occur at 1312 cm^{-1} , 1565 cm^{-1} and 1595 cm^{-1} for the D, G and D' bands, respectively, and the fn.MWCNT–Au_{nano} composite follows the same trend with bands at 1314 cm^{-1} , 1570 cm^{-1} and 1600 cm^{-1} , respectively. In both spectra, the D band is more intense than the G band. This was also evident in the pristine MWCNTs indicating some degree of surface damage during the manufacturing process. The intensity of the peaks is about 20% higher for the fn.MWCNT–Au_{nano} composite and this is consistent with surface enhanced Raman scattering (SERs), which is observed when gold nanoparticles are attached to nanotubes [25,26]. The RAMAN spectrum of SDS was also recorded and a RAMAN shift was observed at 1450 cm^{-1} . It is clear that there is no evidence of this band in Fig. 4 which shows that all the SDS is removed from the composite during the pre-treatment steps.

3.2. Electrochemical detection of glucose

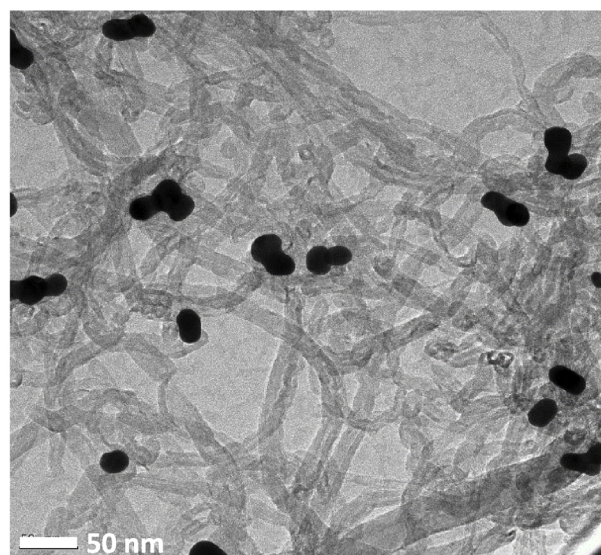
The electrochemical detection of glucose at the fn.MWCNT–Au_{nano} composites was studied using cyclic voltammetry and constant potential amperometry. All studies were carried out in a neutral PBS solution, as this corresponds with physiological pH levels. A concentration range that encompasses both the physiological levels of glucose and the elevated levels of glucose in blood, which typically ranges from 1.0 mM to 20.0 mM, was used. Furthermore, carbon electrodes, glassy carbon and carbon screen printed electrodes, were employed as the substrates. These were selected as the oxidation of glucose does not occur at carbon-based materials, particularly at a neutral pH, and therefore the current obtained can be linked to the supported gold nanoparticles and not the underlying substrate.

Cyclic voltammograms recorded in 0.1 M PBS, at a pH of 7.4, are shown in Fig. 5(a) for glucose concentrations ranging from 1.0 to 10.0 mM for the borohydride system. These data are dominated by the charging capacitance of the carbon nanotubes, which becomes

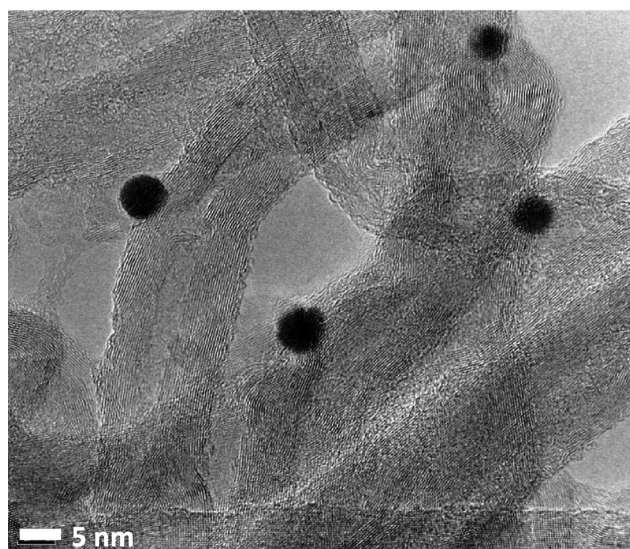
(a)



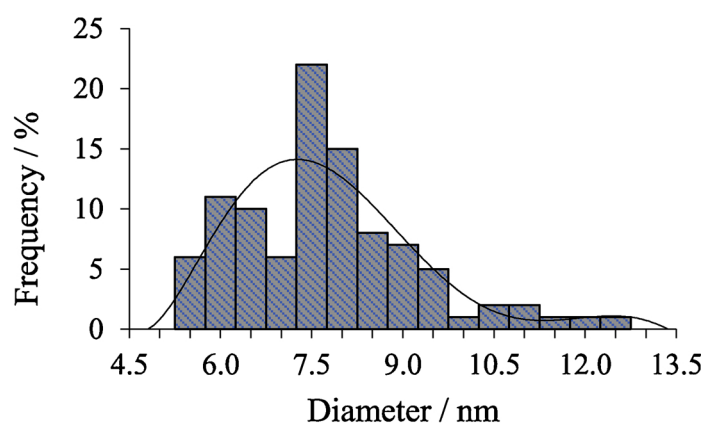
(b)



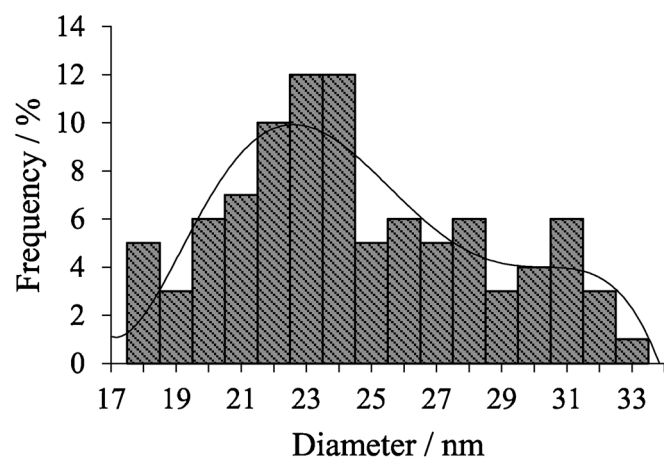
(c)



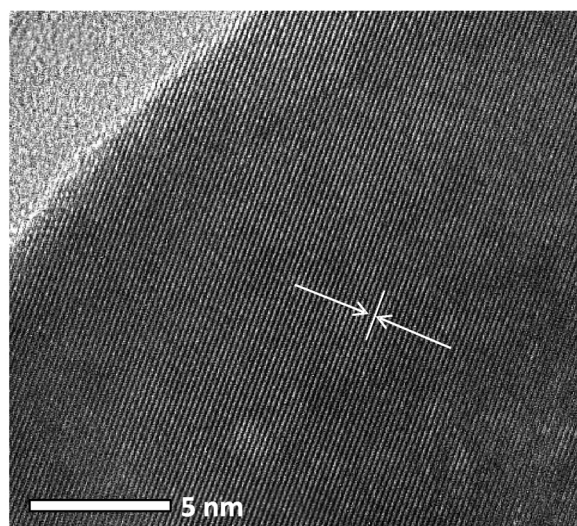
(d)



(e)



(f)



(caption on next page)

Fig. 2. TEM micrographs and size distribution plots for fn.MWCNT–Au_{nano} formed using borohydride (a), (c), (d) and (f) and for fn.MWCNT–Au_{nano} formed using citrate (b) and (e).

increasingly larger as the potential is cycled below 0.0 V vs. SCE. Nevertheless, the oxidation of glucose is seen at approximately 0.18 V vs. SCE in both the forward and reverse cycles. The voltammogram recorded in the absence of glucose (dotted trace) shows that the electrochemistry of gold is evident in the region where the glucose is detected. These voltammograms resemble, to some degree, the data obtained for gold in alkaline solutions [14,17–19]. The first oxidation peak at approximately 0.12 V vs. SCE, seen in the forward direction, has been attributed to the direct electrochemical oxidation of glucose to form the adsorbed intermediates, while the peak at about 0.20 V vs. SCE (again in the forward direction) corresponds to the continuous oxidation of the dehydrogenated glucose to gluconolactone by adsorbed OH[−] species and finally the gluconolactone is converted to gluconate [14]. It is evident from Fig. 5 that these two peaks have similar peak currents, which is different to that observed in alkaline solutions, where the first peak is typically a shoulder peak [14,18]. The lower OH[−] concentration in the neutral buffer gives rise to a significant reduction in this second peak which is dependent on the presence of OH[−] and Au(OH)_{ads}. On the reverse scan the gold oxides, generated during the forward cycle, are reduced and this provides a fresh clean surface for the direct oxidation of glucose, which is seen at about 0.18 V vs. SCE in Fig. 5(a). There is a direct correlation between the concentration of glucose and the peak current observed during the reverse scan, as shown in the linear calibration curve presented in Fig. 5(b).

The cast deposits showed very good adhesion properties and this appears to be related to the pre-treatments employed before the sensor was used. As detailed in the experimental section, the fn.MWCNT–Au_{nano} modified electrodes were cycled in 0.3 M NaOH, followed by the 0.1 M PBS buffer, 1.0 M H₂SO₄ and finally in the 0.1 M PBS buffer. These events will lead to the formation of surface oxides at the carbon substrates and it appears that this surface oxide integrates and binds the nanotubes to the carbon substrate.

The large capacitive currents, Fig. 5(a), have a negative effect on the limit of detection (LOD) and constant potential amperometry was used to minimise this background current. In addition, the system was miniaturised using carbon screen printed electrodes. Again, there was no evidence of glucose oxidation at these carbon electrodes, or indeed at the functionalised carbon nanotubes. The voltammograms recorded using the screen printed electrodes are presented in Fig. 6(a) where the data recorded in the presence of glucose are compared with the plot obtained in 0.1 M PBS. These voltammograms are more capacitive and this can be explained by the higher surface area of the screen printed electrodes and the higher loading of fn.MWCNT–Au_{nano} (5 µL at GC and

10 µL at SPE). The oxidation of glucose is evident during the reverse cycle between 0.05 V and −0.08 V vs. Ag|AgCl. An applied potential of −0.05 V vs. Ag|AgCl was used in the amperometry experiments and this provided the highest current response and corresponds to the oxidation of glucose during the reverse cycle.

A representative calibration curve is shown in Fig. 6(b) while the corresponding amperometric response is shown in the inset for the composite deposited at the SPE electrode. Steady-state current responses were obtained after about 60 s, indicating an efficient response time. The sensitivity was calculated as $2.77 \pm 0.14 \mu\text{A}/\text{mM}$ and a LOD value of 4.1 µM was achieved. Furthermore, a linear calibration curve was obtained between 0.1 mM and 20.0 mM. These data compare reasonably well to some of the reports using alkaline conditions. For example, Kangkamano et al. [14] obtained a LOD value of 0.5 µA and a linear range between 0.001 mM and 0.1 mM, while Zhou et al. [19] achieved a LOD value of 0.5 µA and a linear range between 0.005 mM and 37.0 mM, Fu et al. [16] reported a LOD value of 1.0 µA and a linear range from 10 µA to 6.1 mM and Jeong et al. [15] found a linear range between 2.0 µA and 19.6 mM and a LOD of 0.5 µA. However, the sensitivity found in these alkaline solutions is much higher with values ranging between 0.98 µA/mM to 1989 µA/mM being reported [15,16], illustrating the role of OH[−] ions and Au(OH)_{ads} in promoting the oxidation of glucose.

A higher sensitivity of $4.1 \pm 0.21 \mu\text{A}/\text{mM}$ was obtained using citrate as the reducing agent in forming the gold nanoparticles. However, this composite showed poor stability, as batches of this material only yielded sensitive films for a period of two to three days. This was attributed to aggregation of the gold particles, as the particles were larger, appeared in closer proximity to each other and were present at a higher loading, as illustrated in Fig. 2(b). The higher sensitivity is related to the higher gold loading, indicating that higher amounts of gold facilitate more efficient oxidation of glucose, however the nature of the gold is equally important. For example, on cycling a gold electrode in a neutral 10 mM glucose solution, no glucose oxidation peak was observed and a very poor response was obtained. This illustrates the good catalytic activity of the gold nanoparticles and provided the gold nanoparticles are small and well dispersed along the walls of the carbon nanotubes, good stability is obtained. This is further illustrated in Fig. 7, where the current recorded for a 10.0 mM glucose concentration is shown as a function of the number of times the sensor is used. Between these experiments the sensor was stored in the PBS solution for short periods and then the current was re-measured using constant potential amperometry.

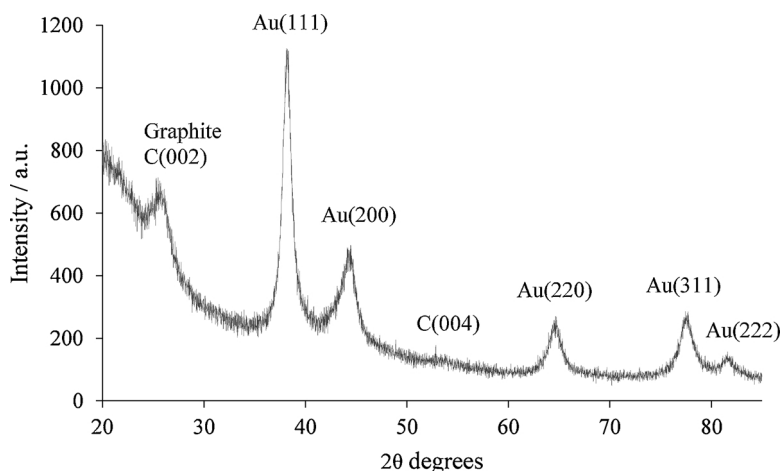


Fig. 3. XRD spectrum of the fn.MWCNT–Au_{nano} composite.

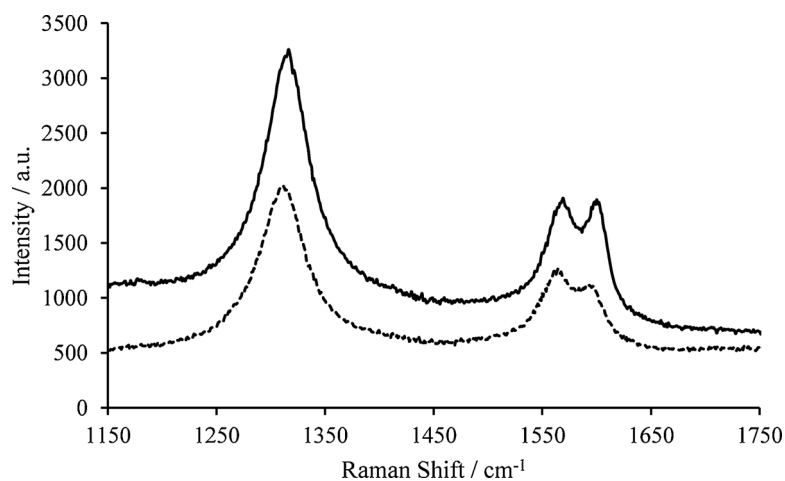


Fig. 4. Raman spectra of ···· the fn.MWCNTs and — the fn.MWCNT-Au_{nano} composite.

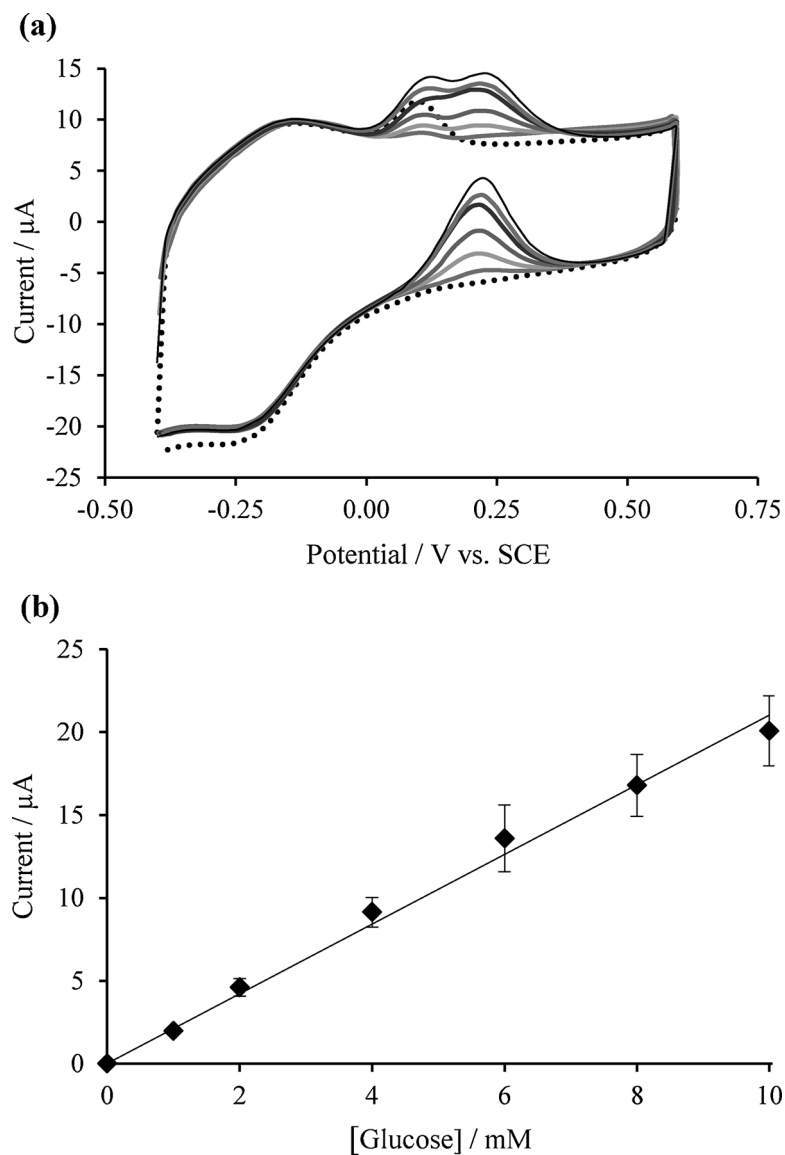


Fig. 5. (a) Cyclic voltammograms recorded at 100 mV s^{-1} in 0.1 M PBS with glucose concentrations between 1.0 and 10 mM and in the absence of glucose (····) for fn.MWCNT-Au_{nano} modified GC electrode and (b) corresponding linear calibration curve (borohydride system).

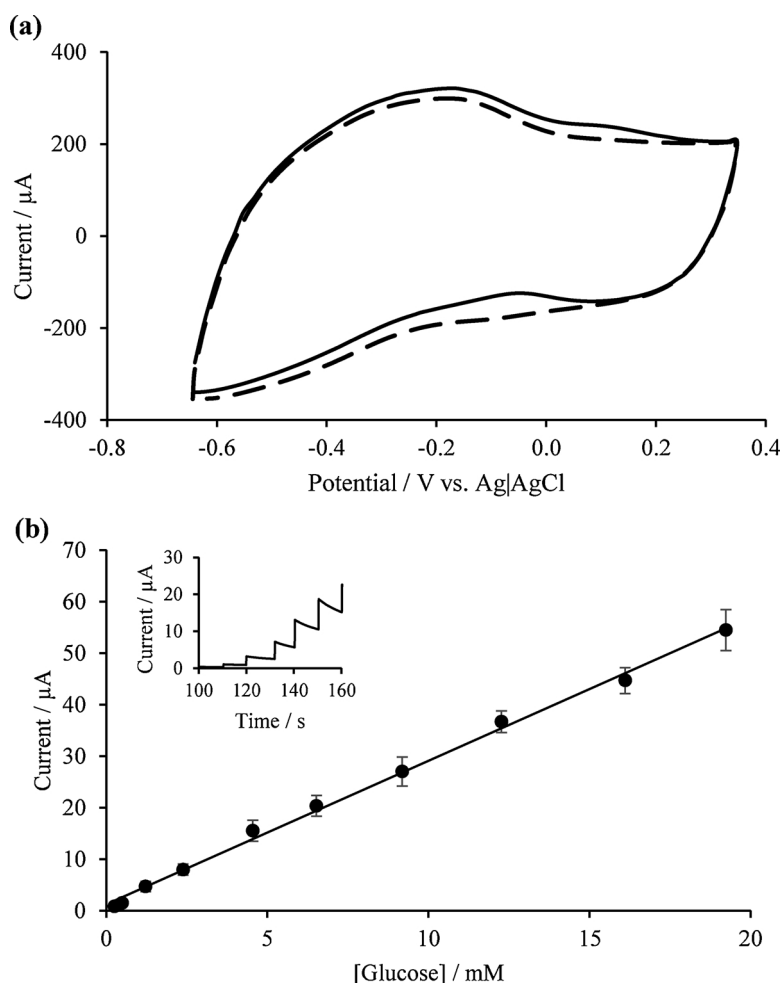


Fig. 6. (a): Cyclic voltammograms recorded at 100 mV s⁻¹ in 0.1 M PBS — with glucose and - - - in the absence of glucose for fn.MWCNT–Au_{nano} deposited at the SPE electrode. (b) Calibration curve and amperometric current plot (inset) recorded for the fn.MWCNT–Au_{nano} modified SPE electrode in 0.1 M PBS (borohydride system).

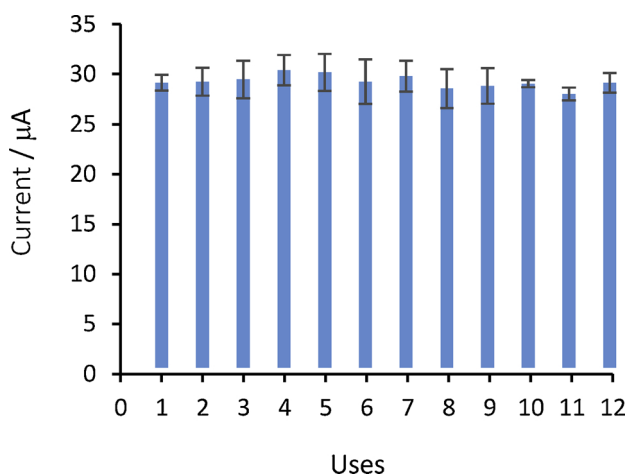


Fig. 7. Current plotted as a function of the number of times the fn.MWCNT–Au_{nano} modified SPE electrode was used in 0.1 M PBS with 10 mM glucose (borohydride system).

The selectivity of the composite sensor was studied using various chemical species that are normally present in blood. The influence of ascorbic acid (AA), which is a well-known interference as it is readily oxidised at a number of electrodes [27] and the products of its oxidation can foul the surface [28], is shown in Fig. 8(a). Aliquots of glucose were added prior to and after the AA injection. The initial concentration

of glucose was set at 4.0 mM and then sufficient AA was added to give 0.1 mM AA and further additions were made to give 0.5 mM. As AA exists at a maximum concentration of 0.1 mM in blood [29], this is the most relevant concentration. There is no evidence of any significant interference from AA, there is only a slight increase in the current on addition of the higher 0.5 mM concentration. On the subsequent addition of glucose, the current increase in response to the added glucose concentration is identical to that observed in the absence of AA. The applied potential of -0.05 V vs. Ag|AgCl used in these amperometry experiments is too negative to enable significant oxidation of AA and there is little or no interference seen.

The potential interference of galactose was studied at 0.33 mM, which corresponds to normal physiological concentrations, at 0.55 mM which indicates elevated levels and 1.0 mM to represent excessively high levels [30]. Again, there was no interference from any of these levels and data similar to Fig. 8(a) were obtained. Likewise, there was no interference from fructose at concentrations of 6.33, 27.75 and 2.75 mM [31]. Some interference was observed with acetaminophen (paracetamol) which is a widely used over-the-counter analgesic and antipyretic that is absorbed into the blood and significantly more interference was evident with uric acid (UA). As shown in Fig. 8(c), there is significant interference from UA, with a considerable reduction in the current on addition of UA. Furthermore, the glucose response is not restored on the subsequent injection of glucose. Uric acid is electro-active and it causes significant fouling at electrode surfaces [32]. The reduction in the glucose current, observed in Fig. 8(c), is consistent with fouling. Although significant oxidation of UA is unlikely at -0.05 V

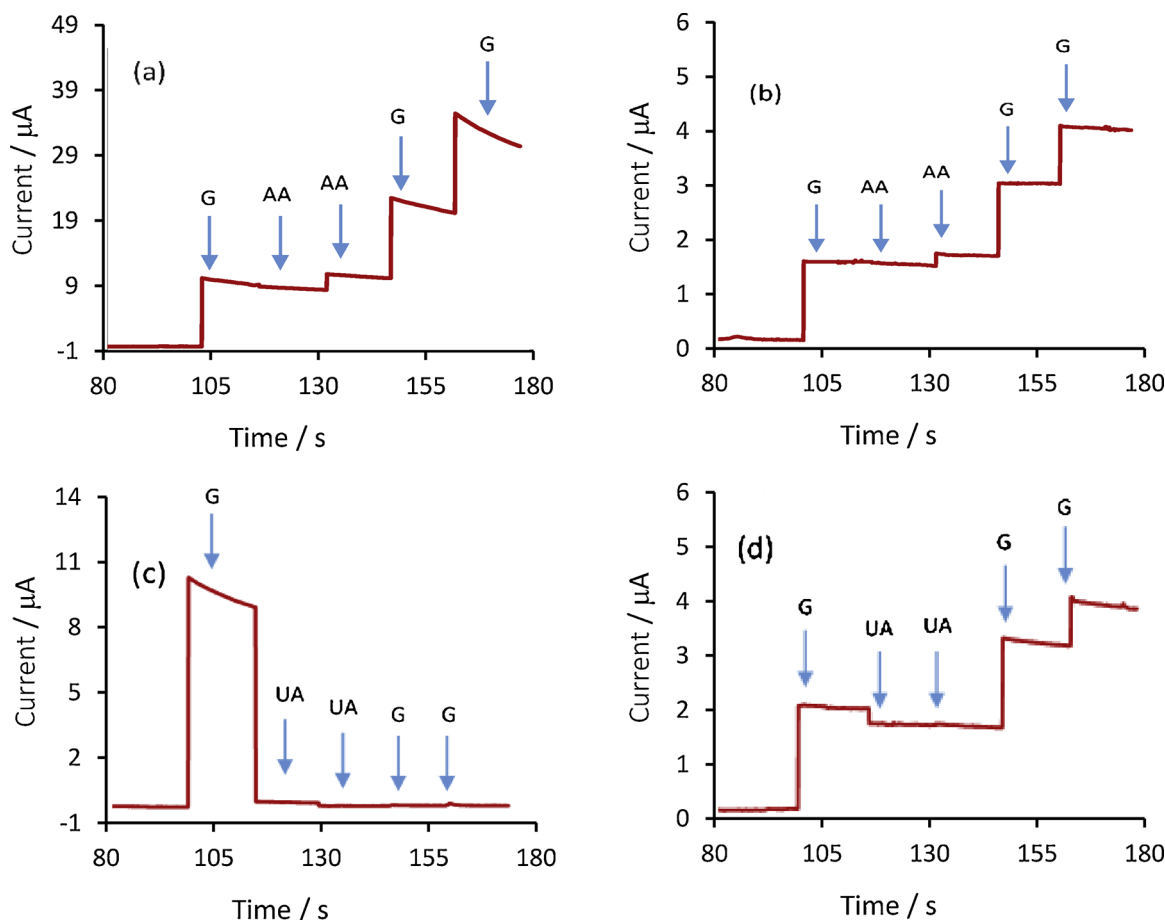


Fig. 8. Amperometric current response in 0.1 M PBS to the addition of AA and UA followed by glucose (G) at the fn.MWCNT–Au_{nano} modified SPE (a) and (c) and at the Nafion[®] modified composite electrodes (b) and (d).

vs. Ag/AgCl and there was negligible UA oxidation at this potential when the composite was used in a UA-containing solution without glucose, the presence of UA in solution and its slight oxidation is sufficient to foul the gold nanoparticles. This effect is different to that observed with AA where a small current increase, consistent with the oxidation of AA, is evident. With UA, the irreversible oxidation of the molecule gives a low oxidation current, while fouling gives rise to a more significant reduction in the glucose oxidation current as a clean gold surface can no longer be generated on reduction of the gold oxide/hydroxide. Although the carbon nanotubes were functionalised with carboxylate groups, the concentration of these negatively charged groups at about 6% is not sufficient to repel the anionic urate.

It was possible to eliminate these interferences by modifying the composite with Nafion[®], which is well known for its ability to repel anionic species, such as urate and ascorbate [33]. Representative data for the composite modified with Nafion[®] are shown in Fig. 8(b) and (d) and clearly illustrate the selectivity provided by the Nafion[®] layer in the presence of uric acid. However, by adding this layer, the steady-state currents are significantly reduced, as evident from a comparison of Fig. 8(a) and (b) or Fig. 8(c) and (d). This in turn reduces the sensitivity of the Nafion[®] modified composites. The sensitivity was reduced to 0.55 $\mu\text{A}/\text{mM}$ and the LOD was increased to 10.0 μA . This may be related to a reduction in the rate of diffusion of the glucose molecules across the Nafion[®] barrier. Nevertheless, a linear calibration curve was achieved as illustrated in Fig. 9. Although the LOD value is increased, the linear range extends from 0.1 mM to 25 mM glucose and this encompasses the typical glucose levels reported for diabetic patients, which can vary from 2 mM to 25 mM [34].

The shelf-life of the sensor was monitored by recording the response

of the composite to 10.0 mM glucose after it was stored for various time periods in air. The data obtained for the composite and the Nafion[®] coated composite are shown in Fig. 10. It is clear from these data, that the composite is stable for several days and the additional Nafion[®] layer adds to this stability. Although it is possible to detect glucose after 35 days, the current begins to decay from the original value after approximately 14 days. While the Nafion[®] layer reduces the sensitivity, it is essential in the elimination of interferences when the sensor is used at physiological pH and it also enhances the overall stability of the composite.

4. Conclusion

Carbon nanotubes decorated with gold nanoparticles were dispersed and cast onto a glassy carbon electrode and onto carbon screen printed electrodes and used to detect glucose in a neutral phosphate buffer solution. The gold nanoparticles were formed within 5 min using sodium borohydride as a reducing agent. The nanoparticles were well dispersed along the carbon nanotubes with an average diameter of 7.5 nm and with a gold loading of 2.0%. Although the carbon nanotubes have a high capacitance and this was clearly evident using cyclic voltammetry, the oxidation of glucose was observed during the forward and the reverse cycles. Constant potential amperometry was used to detect glucose. The optimum potential corresponds well with the potential where the reduction of gold oxides occurs giving an oxide-free surface for the direct oxidation of glucose. A linear calibration curve was obtained giving a sensitivity of $2.77 \pm 0.14 \mu\text{A}/\text{mM}$, a limit of detection of 4.1 μA and a linear region extending beyond 20.0 mM. Very good selectivity was observed in the presence of ascorbic acid,

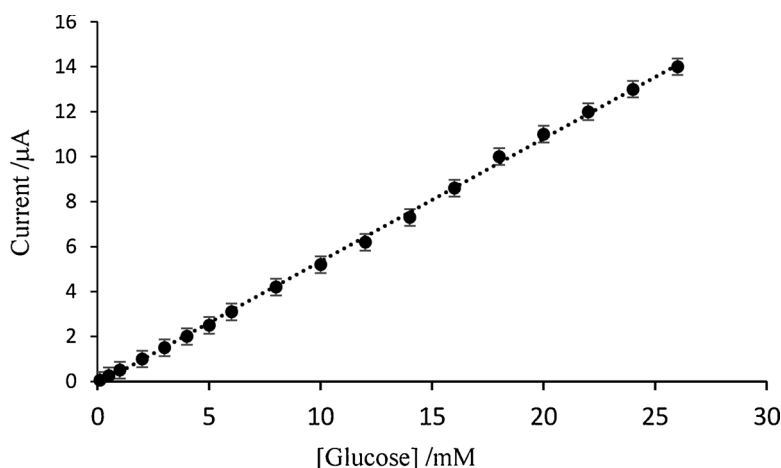


Fig. 9. Calibration curve recorded for the Nafion[®] modified fn.MWCNT-Au_{nano} SPE in 0.1 MPBS at a pH of 7.4.

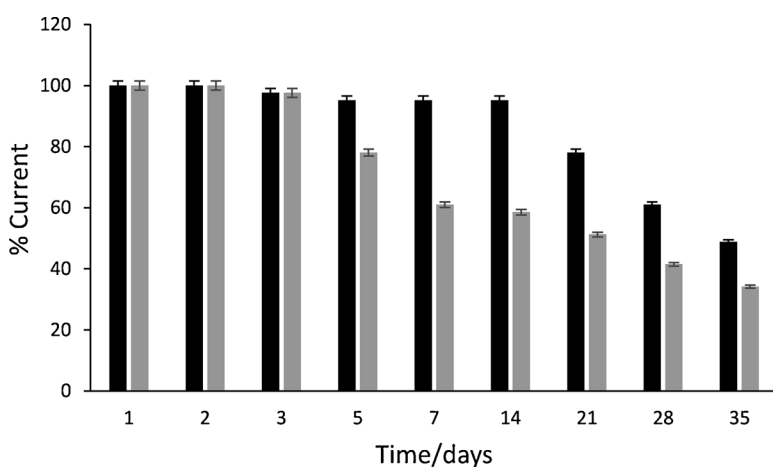


Fig. 10. Amperometric response (expressed as a % of the original current) for the — fn.MWCNT-Au_{nano} modified SPE and the — Nafion[®] modified composite in 0.1 M PBS with 10 mM glucose as a function of the storage time in air.

fructose and galactose. The addition of uric acid showed evidence of significant interference but this was eliminated successfully by coating the composites with a Nafion[®] film. While this added film reduced the sensitivity of the composite, a linear range extending from 0.1 mM to 25 mM was observed, which covers the normal and elevated glucose levels in blood. This permselective barrier is essential when the composite electrode is used at physiological pH. Very good stability was achieved when the sensor was stored in air. This was attributed to the well dispersed gold nanoparticles that prevent agglomeration of the particles and the presence of the Nafion[®] layer.

Acknowledgement

D. Branagan would like to thank Kildare County Council for a scholarship to undertake this work.

References

- [1] R. Prehn, M. Cortina-Puig, F.X. Munoz, A non-enzymatic glucose sensor based on the use of gold micropillar array electrodes, *J. Electrochemical Society* 159 (2012) F134–F139.
- [2] G.G. Guilbault, G.J. Lubrano, Enzyme electrode for the amperometric determination of glucose, *Anal. Chim. Acta* 64 (1973) 439–455.
- [3] S. Park, H. Boo, T.D. Chung, Electrochemical non-enzymatic glucose sensors, *Anal. Chim. Acta* 556 (2006) 46–57.
- [4] A. Sun, J. Zheng, Q. Sheng, A highly sensitive non-enzymatic glucose sensor based on nickel and multi-walled carbon nanotubes nanohybrid films fabricated by one-step co-electrodeposition in ionic liquids, *Electrochim. Acta* 65 (2012) 64–69.
- [5] J.M. Harris, C. Reyes, P.G. Lopez, Common causes of glucose oxidase instability in *in vivo* biosensing: a brief review, *J. Diabetes Sci. Technol.* 7 (4) (2013) 1030–1038.
- [6] M. Zayats, E. Kratz, I. Willner, Electrical contacting of glucose oxidase by surface-reconstitution of the apo-protein on a relay-boronic acid-FAD cofactor monolayer, *J. Am. Chem. Soc.* 124 (2002) 2120–2121.
- [7] M. Pasta, F. La Mantia, Y. Cui, Mechanism of glucose electrochemical oxidation on gold surface, *Electrochim. Acta* 55 (2010) 5561–5568.
- [8] M. Tominaga, M. Nagashima, K. Nishiyama, I. Taniguchi, Surface poisoning during electrocatalytic monosaccharide oxidation reactions at gold electrodes in alkaline medium, *Electrochem. Commun.* 9 (2007) 1892–1898.
- [9] Y. Li, Y.-Y. Song, C. Yang, X.-H. Xia, Hydrogen bubble dynamic template synthesis of porous gold material for nonenzymatic electrochemical detection of glucose, *Electrochem. Commun.* 9 (2007) 981–988.
- [10] C. Guo, Y. Wang, Y. Zhao, C. Xu, Non-enzymatic glucose sensor based on three dimensional nickel oxide for enhanced sensitivity, *Anal. Methods* 5 (5) (2013) 1644–1647.
- [11] W. Wang, Z. Li, W. Zheng, J. Wang, H. Zhang, C. Wang, Electrospun palladium (IV)-doped copper oxide composite nanofibers for non-enzymatic glucose sensors, *Electrochem. Commun.* 11 (2009) 1811–1814.
- [12] S. Park, D.T. Chung, H.C. Kim, Nonenzymatic glucose detection using mesoporous platinum, *Anal. Chem.* 75 (2003) 3046–3049.
- [13] M. Gougis, A. Tabet-Aoul, D. Ma, M. Mohamedi, Laser synthesis and tailor-design of nanosized gold onto carbon nanotubes for non-enzymatic electrochemical glucose sensor, *Sens. Actuators B: Chem.* 193 (2014) 363–369.
- [14] T. Kangkamano, A. Numuam, W. Limbut, P. Kanatharana, P. Thavarungkul, Chitosan cryogel with embedded gold nanoparticles decorated multiwalled carbon nanotubes modified electrode for highly sensitive flow based non-enzymatic glucose sensor, *Sens. Actuators B: Chem.* 246 (2017) 854–863.
- [15] H. Jeong, D.M. Nguyen, M.S. Lee, H.G. Kim, S.C. Ko, L.K. Kwac, N-doped graphene-carbon nanotube hybrid networks attaching with gold nanoparticles for glucose non-enzymatic sensor, *Mater. Sci. Eng. C* 90 (2018) 38–45.
- [16] S. Fu, G. Fan, L. Yang, F. Li, Non-enzymatic glucose sensor based on Au nanoparticles decorated ternary Ni–Al layered double hydroxide/single-walled carbon nanotubes/graphene nanocomposite, *Electrochim. Acta* 152 (2015) 146–154.
- [17] I.G. Casella, M. Contursi, R. Toniolo, A Non-enzymatic carbohydrate sensor based on multiwalled carbon nanotubes modified with adsorbed active gold particles, *Electroanalysis* 26 (2014) 988–995.
- [18] H. Zhu, X. Lu, M. Li, Y. Shao, Z. Zhu, Nonenzymatic glucose voltammetric sensor based on gold nanoparticles/carbon nanotubes/ionic liquid nanocomposite, *Talanta* 79 (2009) 1446–1453.

- [19] L. Zhou, T. Gan, D. Zheng, J. Yan, C. Hu, S. Hu, High-density gold nanoparticles on multi-walled carbon nanotube films: a sensitive electrochemical nonenzymatic platform of glucose, *J. Exp. Nanosci.* 7 (2012) 263–273.
- [20] Z. Wang, M.D. Shirley, S.T. Meikle, R.D.L. Whitby, S.V. Mikhlovsky, The surface acidity of acid oxidised multi-walled carbon nanotubes and the influence of in-situ generated fulvic acids on their stability in aqueous dispersions, *Carbon* 47 (2009) 73–79.
- [21] R. Sreeja, P.M. Aneesh, K. Hasna, K.M. Jayaraj, Linear and nonlinear optical properties of multi walled carbon nanotubes with attached gold nanoparticles, *J. Electrochemical Society* 158 (2011) K187–K191.
- [22] X. Hou, L. Wang, X. Wang, Z. Li, Coating multiwalled carbon nanotubes with gold nanoparticles derived from gold salt precursors, *Diam. Relat. Mater.* 20 (2011) 1329–1332.
- [23] B.D. Cullity, *Elements of X-Ray Diffraction*, Addison-Wesley, 1956.
- [24] I.D. Rosca, F. Watari, M. Uo, T. Akaska, Oxidation of multiwalled carbon nanotubes by nitric acid, *Carbon* 43 (2005) 3124–3131.
- [25] A.I. Lopez-Lorente, B.M. Simonet, M. Valcarcel, B. Mizaikoff, Bare gold nanoparticles mediated surface-enhanced Raman spectroscopic determination and quantification of carboxylated single-walled carbon nanotubes, *Anal. Chim. Acta* 788 (2013) 122–128.
- [26] T. Assmus, K. Balasubramanian, M. Burghard, K. Kern, M. Scolari, N. Fu, A. Myalitsin, A. Mews, Raman properties of gold nanoparticle-decorated individual carbon nanotubes, *Appl. Phys. Lett.* 90 (2007) 173109.
- [27] X. Zhang, J. Ju, J. Wang, *Electrochemical Sensors, Biosensors and Their Biomedical Applications*, Academic Press, 2011.
- [28] S.M. Tan, H.L. Poh, Z. Sofer, M. Pumera, Boron-doped graphene and boron-doped diamond electrodes: detection of biomarkers and resistance to fouling, *Analyst* 138 (17) (2013) 4885–4891.
- [29] M.D. Rubianes, G.A. Rivas, Carbon nanotubes paste electrode, *Electrochem. Commun.* 5 (2003) 689–694.
- [30] K. Weidemaier, A. Lastovich, S. Keith, J.B. Pitner, M. Sistare, R. Jacobson, D. Kurisko, Multi-day pre-clinical demonstration of glucose/galactose binding protein-based fiber optic sensor, *Biosens. Bioelectron.* 26 (2011) 4117–4123.
- [31] L.M.D. Delbridge, V.L. Benson, R.H. Ritchie, K.M. Mellor, Diabetic cardiomyopathy: the case for a role of fructose in disease etiology, *Diabetes* 65 (12) (2016) 3521–3528.
- [32] S. Jesny, K.K. Girish, Electrocatalytic resolution of guanine, adenine and cytosine along with uric acid on poly (4-amino-3-hydroxy naphthalene-1-sulfonic acid) modified glassy carbon electrode, *J. Electroanal. Chem.* 801 (2017) 153–161.
- [33] A. Liao, P. Li, H. Zhang, M. Guo, Y. Xia, Z. Li, W. Huang, Highly Sensitive Determination of 4-Nitrophenol at a Nafion Modified Glass Carbon Nanofilm Electrode, *J. Electrochem. Soc.* 164 (2) (2017) H63–H69.
- [34] S.A. Zaidi, J.H. Shin, Recent developments in nanostructure based electrochemical glucose sensors, *Talanta* 149 (2016) 30–42.